

# The properties of ZnS thin films prepared by rf-magnetron sputtering from nanoparticles synthesized by solvothermal/hydrothermal route

R. Mendil<sup>1</sup> · Z. Ben Ayadi<sup>1</sup> · J. Ben Belgacem<sup>1</sup> · K. Djessas<sup>2,3</sup>

Received: 18 May 2015 / Accepted: 7 September 2015 / Published online: 15 September 2015  
© Springer Science+Business Media New York 2015

**Abstract** Zinc Sulfide (ZnS) has been proposed as a novel buffer layer, alternative to CdS for solar cell applications. ZnS thin films were deposited by rf-magnetron sputtering using, nanocrystalline powder synthesized by solvothermal/hydrothermal route. ZnS nanoparticles with a grain size between 10 and 20 nm were obtained by simple solvothermal/hydrothermal technique. The powders as synthesized were used to develop the buffer layers of nanostructured ZnS by rf-magnetron sputtering. The structural, surface morphology and optical properties of the films were studied. The as-deposited ZnS films were polycrystalline textured and a very smooth surface was obtained. The films are highly transparent in the visible wavelength region with a transmittance higher than 85 %.

## 1 Introduction

ZnS is one of the most important direct wide-band gap semiconductor materials of the II–VI group. It has traditionally shown remarkable fundamental properties versatility and a promise for novel diverse applications, including light-emitting diodes [1], electroluminescence

[2], flat panel displays [3], lasers [4] and buffer layers for thin film solar cells [5, 6]. As an important semiconductor, ZnS is mostly found in one of two structural forms, cubic or hexagonal which have wide-band gaps of 3.54 and 3.80 eV respectively at room temperature [7]. It has a high refractive index and a high transmittance in the visible region [8, 9].

ZnS thin films have been proven to play a crucial role in photovoltaic and optoelectronic devices. Generally CdS is one of the most extensively used material as a buffer layer in solar cells based on CdTe and Cu(Ga,In)(S,Se)<sub>2</sub> absorber layers [10, 11]. However, due to the toxic hazards with respect to the production and use of CdS layers, much attention has been focused on developing Cd-free buffer layers. One such possible replacement of CdS is ZnS, which has been primarily investigated as a buffer layer in ZnO/ZnS/Cu(Ga,In)(S,Se)<sub>2</sub> devices [12, 13]. CIGS based thin film solar cells with a ZnS buffer layer achieved a high conversion efficiency of 17.4 % [14]. Compared with conventionally used CdS buffer layer, ZnS would be advantageous because it is nontoxic, more efficient, relatively cheaper and abundant and they have good transparency.

ZnS thin films have been mainly prepared by molecular beam epitaxy (MBE) [15], atomic layer epitaxy (ALE) [16], high pressure sputtering [17] and metal organic chemical vapor deposition (MOCVD) [18]. Most of these techniques involve the use of either sophisticated deposition facilities, increasing the fabrication costs, or use toxic gases like H<sub>2</sub>S. Therefore, keeping in view the importance of alternate buffer layers and the process of their synthesis for heterojunction solar cells, we investigate, in the present study and for the first time, as a buffer material, ZnS prepared by rf-magnetron sputtering based nanocrystalline particles elaborated by solvothermal/hydrothermal route.

✉ R. Mendil  
radia.mendil@yahoo.fr

<sup>1</sup> Laboratoire de Physique des Matériaux et des Nanomatériaux appliquée à l'Environnement, Faculté des Sciences de Gabès, Université de Gabès, Cité Erriadh Manara Zrig, 6072 Gabès, Tunisia

<sup>2</sup> Laboratoire Procédés, Matériaux et Energie Solaire (PROMES-CNRS), TECNOSUD, Rambla de la thermodynamique, 66100 Perpignan, France

<sup>3</sup> Université de Perpignan Via Domitia, 52 Avenue Paul Alduy, 68860 Perpignan Cedex 9, France

This is an attractive technique because sputtering technique performs high deposition rate at room temperature, with no toxic gas emissions, suitable for producing high quality films, easy to expand to large scale glass substrates, low-cost and simple method. On the other hand, materials prepared by solvothermal/hydrothermal technique are of high purity, homogeneous, much less expensive and well adapted for large area applications. Most researchers have used sintered ceramic as a target material in sputtering.

In this paper, the structural and the optical properties of the sputtered ZnS thin films, from nanopowders prepared by different methods were studied and reported.

## 2 Experimental details

All chemicals used in this work were of analytical grade or of highest purity available, without further purification.

### 2.1 Preparation of ZnS nanopowder

ZnS was synthesized by a simple solvothermal/hydrothermal route. Zinc nitrate ( $\text{Zn}(\text{NO}_3)_2 \cdot 6\text{H}_2\text{O}$ ) was employed as the zinc source. Thiourea ( $\text{NH}_2\text{CSNH}_2$ ) was chosen as the sulfur source in the experiments because it can dissolve and release  $\text{S}^{2-}$  ions in aqueous solution at elevated temperatures. Zinc and sulfur sources were taken in 1:1 molar ratios. Ethylenediamine (EN) and deionized water (W) were used as solvents in the different sets of experiments. In each synthesis, the precursors were dissolved in 200 ml of the solvent (EN/W) with vigorous stirring until obtention of homogenized solution. The resulting mixture was transferred into a 1 l autoclave with an addition of 200 ml of the same solvent and maintained at 200 °C for 24 h and then cooled down at room temperature. The obtained white solid product was collected by filtration then washed several times with deionized water followed by absolute ethanol and dried at 70 °C for 4 h.

### 2.2 Thin films deposition

The ZnS thin films with a thickness of about 300 nm were deposited on glass substrate from nanoparticles elaborated by solvothermal/hydrothermal route as described previously using rf-magnetron sputtering technique, with rf generator operating at 13.56 MHz (Cezar rf-power Generator). The sputtering chamber was evacuated to a base pressure of about  $10^{-5}$  mbar. After introducing the sputtering Argon gas with high purity (99.9999 %), the sputtering deposition was carried out at a pressure of  $10^{-3}$  mbar. The sputtering targets were fabricated by taking a suitable aluminum holder, with 50 mm diameter and compacting the ZnS nanopowder. The 1 mm thick glass

substrates (microscope slides) were ultrasonically cleaned in HCl, rinsed in deionized water, then subsequently in ethanol and rinsed again. During the sputtering process, the rf-power was maintained at 40 W and the target-to-substrate distance was fixed at 75 mm. The substrate temperatures during the deposition were fixed at room temperature and 200 °C.

### 2.3 Characterization techniques

The structural, morphological and optical properties were studied in this work. The crystal structure was characterized by X-ray diffraction using  $\text{CuK}\alpha$  radiation (1.5406 Å). The crystallite size has been calculated from XRD data using Scherrer's formula. The composition studies were done by energy dispersive X-ray spectroscopy (EDS) using a scanning electron microscope JEOL, JSM 5410 type with a probe. The ZnS nanopowders as prepared in the first step were also characterized using JEM-200CX transmission electron microscopy (TEM). Surface morphology and roughness were measured using NT-MDT atomic force microscopy (AFM, SMENA) in the tapping mode. The Raman spectroscopy was performed at room temperature using a Raman spectrometer (LABRAM HR-800) with a 488 nm Helium laser line as an excitation source. The experiments were repeated several times to confirm our result.

The optical transmittance of the films was determined using Shimadzu UV-3101 PC spectrophotometer in the wavelength range from 200 to 3000 nm. For transmittance measurement, the beam was made to enter the film through the glass substrate and a blank glass slide was kept in the path of the reference beam for compensation.

## 3 Results and discussion

Figure 1 shows the XRD patterns of the nanoparticles as elaborated in the first step in different solvents (EN/W). The XRD pattern of the product obtained in W indicates the formation of predominantly cubic sphalerite phase of ZnS, according to the JCPDS card number 05-0566, but the presence of the wurtzite phase is also evident. In contrast, the XRD pattern of the product obtained in EN is indexed to the hexagonal wurtzite phase of ZnS (JCPDS, card no. 75-1534). The several peaks of hexagonal phase of ZnS powder have been obtained due to diffraction from (100), (002), (101), (102), (110), (103) and (112) planes of ZnS.

Generally, bulk wurtzite is metastable relative to the cubic phase below 1020 °C. Here, in solvothermal conditions, stable wurtzite ZnS nanostructures are formed at much lower temperatures (200 °C). Although the exact mechanism behind this stabilization is not clear, it is

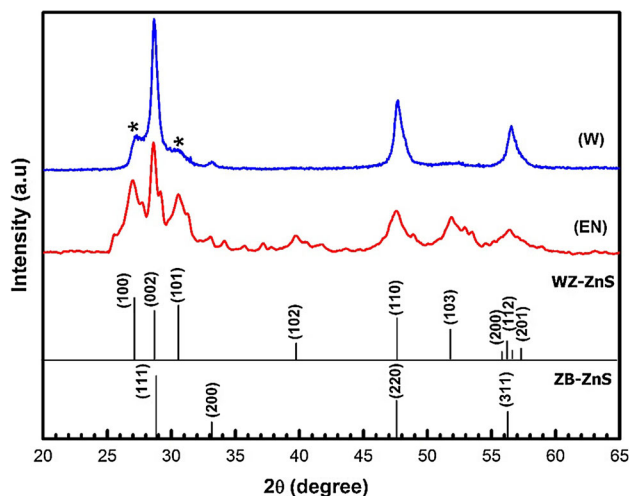


**Fig. 1** XRD patterns of the products ZnS nanoparticles obtained in different solvents. The peaks marked with “\*” correspond to wurtzite structure

supposed that organic molecules of ethylenediamine that can form some intermediate complex with ZnS decompose to produce phase pure wurtzite ZnS [19]. On the other hand, the presence of the wurtzite phase along with the cubic phase in the hydrothermal growth of ZnS (in water) is attributed to the grain growth under pressure in hydrothermal conditions [20].

XRD patterns shown in Fig. 1 are indexed into cubic phase with the calculated lattice constant  $a = 0.538$  nm, and the wurtzite phase ZnS with calculated lattice constants  $a = 0.382$  nm and  $c = 0.624$  nm, respectively, in a good agreement with the reported data (JCPDS, card nos. 05-0566 and 75-1534).

The full width at half-maximum (FWHM) can be used to estimate the average grain size of nanoparticles, according to the Scherrer’s formula [21]:

$$G = \frac{0.9\lambda}{\beta \cos \theta_B} \quad (1)$$

where  $\lambda$  is the X-ray wavelength (1.5406 Å),  $\theta_B$  is the Bragg diffraction angle and  $\beta$  is the FWHM of the XRD peak (in radians). After a correction for the instrumental broadening, an average value of crystallites was found to be 10 and 18 nm for hydrothermal and solvothermal ZnS, respectively.

In order, to confirm the composition of the ZnS powders, EDS analysis was performed. The composition characteristics of the samples reported in Table 1 show that the as-fabricated nanoparticles are composed of Zn and S elements without other impurities. It was seen that, the S/Zn atomic ratio in nanoparticles was lesser than one. It means that there was deficiency of S inside the nanopowders. Figure 2 depicts the TEM images of the ZnS

**Table 1** Atomic compositions of the ZnS nanoparticles and films

	Nanoparticles	Films	
		RT	200 °C
ZnS (W)			
Zn (at.%)	55.85	57.72	50.40
S (at.%)	44.15	42.28	49.60
S/Zn	0.79	0.74	0.98
ZnS (EN)			
Zn (at.%)	55.26	56.39	51.41
S (at.%)	44.74	43.61	48.59
S/Zn	0.81	0.77	0.95

nanoparticles synthesized by solvothermal and hydrothermal route. TEM images for the samples synthesized with the solvent water reveal that the product only contains ZnS nanoparticles with sphalerite shape with a size of 10 nm, which is consistent with the result of XRD spectra, as shown in Fig. 2a. The high-resolution TEM (HRTEM) provides further insights into the structure of ZnS nanoparticles. Figure 2c represents HRTEM image of ZnS (hydrothermal). The measured fringe spacing of the crystalline is 0.312 nm corresponding to the (111) planes of the cubic ZnS, indicating that the nanoparticles grows along the [111] orientation. When EN was used as solvent, the resultant ZnS material is mostly composed of nanoparticles with few nanorods (Fig. 2b).

In Fig. 3, we report the XRD patterns of the thin films deposited onto glass substrates by rf-magnetron sputtering at room temperature (RT) and 200 °C using ZnS nanocrystalline powder synthesized by different solvents (W and EN). The patterns show that all films exhibited most intense peak at  $2\theta = 28.6^\circ$  which indicates that the samples are strongly oriented, which corresponds either to the hexagonal (002) or the cubic (111) reflection. While films sputtered at room temperature have a slight peaks centered at  $2\theta = 47.3^\circ$  which can be attributed to (220) or (110) plane of cubic or hexagonal phase of ZnS, respectively. Similar observations have been reported for ZnS thin films grown by close-spaced evaporation [22] and magnetron sputtering from metallic targets [23, 24].

It suggests that the films sputtered at room temperature are less preferentially oriented than the sample sputtered at 200 °C. XRD results indicate that the growth temperature influences the crystalline phases of ZnS films deposited on glass substrates. Some authors have reported that low temperature (<350 °C) growth of ZnS results in a cubic structure for the thin films [25, 26]. In the case of sample (a), the XRD pattern shows the emergence of new additional peak at  $2\theta = 27.6^\circ$  which can be attributed to (100)

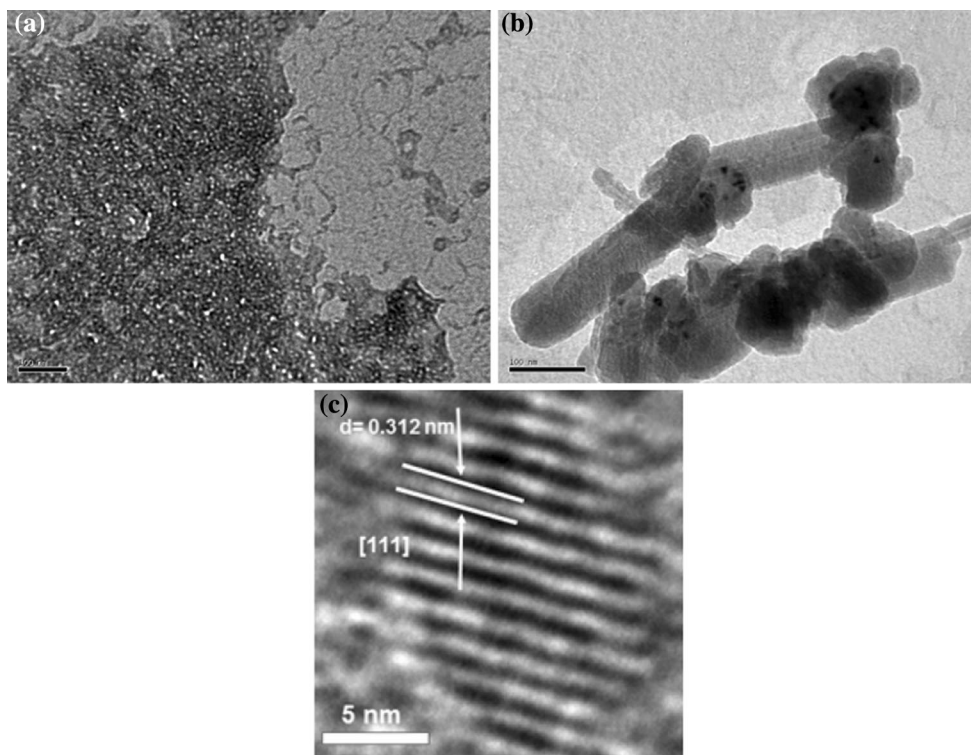


**Fig. 2** TEM images of ZnS nanoparticles synthesized by hydrothermal (a) and solvothermal (b) route. HRTEM image of ZnS synthesized by hydrothermal route (c)

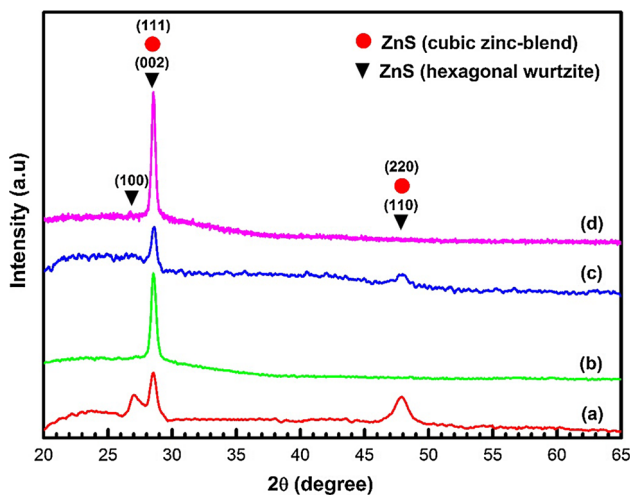


**Fig. 3** XRD patterns of ZnS thin films deposited at RT (a, c) and 200 °C (b, d) from nanoparticles elaborated by hydrothermal (a, b) and solvothermal (c, d), respectively

plane of hexagonal of ZnS. Similar observation reported by Yoo et al. [23] in the case of ZnS thin film.

It is also clearly observed that, the intensity of the (002) or (111) XRD peak increases with increasing the substrate temperature. On the other hand, as seen in Table 2, the FWHM decreases with increasing the substrate temperature.

Since the FWHM of the (002) or (111) diffraction peak is inversely proportional to the grain size of the film, then the grain size of ZnS thin films increases with increasing the substrate temperature (Table 2). The grain sizes for the films, calculated using Scherrer’s formula, from the intensity of (002) or (111) XRD peak, are smaller to those of the ZnS powder for films deposited at RT and increased at 200 °C (see Table 2).

The chemical composition of the films have been estimated by EDS analysis (Fig. 4) and reported in Table 1. According to Table 1, EDS analysis shows some difference in the ratio of sulfur and zinc in ZnS thin films deposited at RT on glass substrates. EDS shows the presence of an excess of Zn for films. Such excess of Zn as impurity is likely due to unreacted  $Zn^{2+}$  during film deposition at RT. However, the S/Zn ratio is close to unity for the samples elaborated at 200 °C. This implies that the films synthesized at 200 °C bear acceptable stoichiometry.

Figure 5 shows a 3D AFM images in  $5 \mu m \times 5 \mu m$  of ZnS thin films for different annealing conditions. The films deposited at room temperature from nanopowders synthesized by solvothermal/hydrothermal route, shows a uniform grain size distribution and a smooth surface with a maximum height of the surface approximately 23 nm. The root mean square (RMS) values of the surface roughness of the film are given in Table 2. The RMS of the film is about

**Table 2** FWHM ( $\beta$ ), grain size (G), root mean square (RMS) and optical band gap ( $E_g$ ) of ZnS thin films studied in this work

Sample	Target	Growth temperature	$\beta$ (rad)	G (nm)	RMS (nm)	$E_g$ (eV)
(a)	ZnS (W)	RT	0.109	13.01	0.46	4.07
(b)		200 °C	0.070	20.42	1.18	4.38
(c)	ZnS (EN)	RT	0.090	15.88	1.27	4.36
(d)		200 °C	0.061	23.44	43.70	4.38

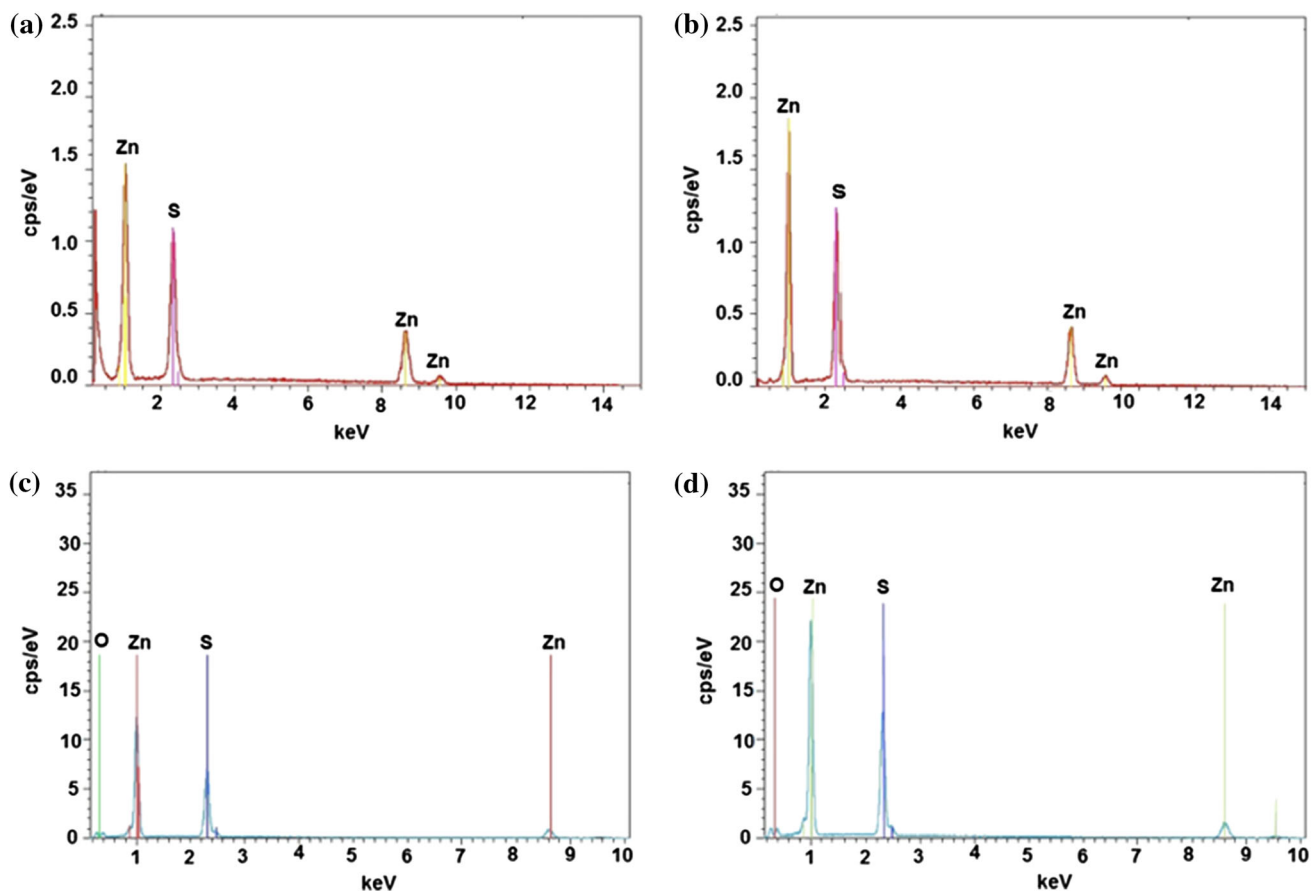


**Fig. 4** EDS spectra of ZnS thin films deposited at RT (a, b) and 200 °C (c, d) from nanoparticles elaborated by hydrothermal (a, c) and solvothermal (b, d), respectively

1 nm. Obviously, the RMS values increased with the increasing substrate temperature. This is due to the fact that with the increasing substrate temperature, the grain size increases and surface morphology becomes rougher. The RMS of the surface roughness of films synthesized by hydrothermal route is about 2 nm for substrate temperature at 200 °C. However, we find a sharp increase in roughness (RMS  $\sim$ 40 nm) and in a maximum height of the surface ( $\sim$ 255 nm) is observed from the film prepared from powder synthesized by solvothermal route.

Raman scattering measurements provide structural features that can be explained to take into account some details of film microstructures. The Raman spectra of ZnS thin films deposited at different substrate temperatures (RT

and 200 °C), in the spectral range from 50 to 1500  $\text{cm}^{-1}$ , are presented in Fig. 6. In general, the transverse optical (TO) and longitudinal optical (LO) modes are positioned at 276 and 351  $\text{cm}^{-1}$ , respectively, for bulk ZnS compound [27]. The locations of the Raman peaks for (a)–(d) samples are presented in Table 3. In the present study, the peaks at 340 and 549  $\text{cm}^{-1}$ , can be identified as LO and 2TO modes, respectively. The presence of the Raman peak at 340  $\text{cm}^{-1}$  can be assigned as the LO mode of cubic ZnS [28]. In fact, the absence of any peak around 72 and 286  $\text{cm}^{-1}$  in the Raman spectra of the present nanostructured ZnS sample suggests that the films have (111) a-axis preferred orientation [29]. The peak at 790  $\text{cm}^{-1}$  observed in the Raman spectra of the present samples corresponds to

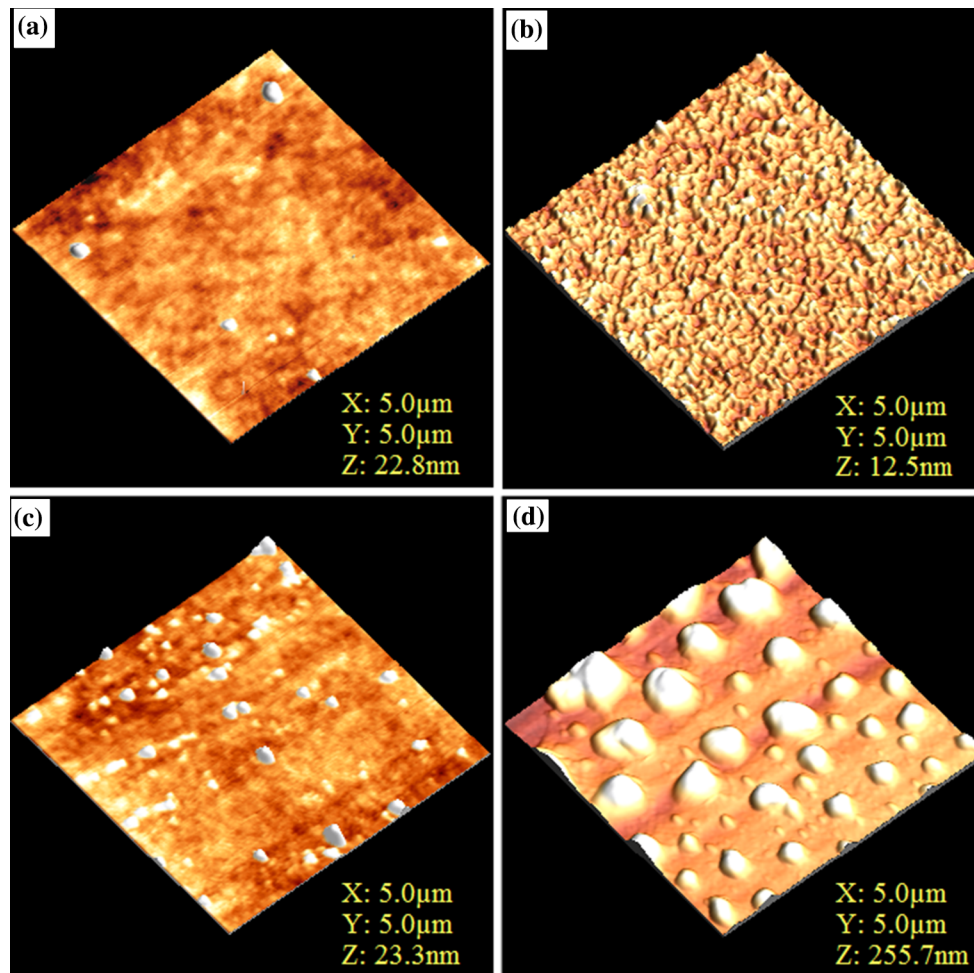


**Fig. 5** AFM surface topology of thin films prepared at RT (a, c) and 200 °C (b, d) from nanoparticles elaborated by hydrothermal (a, b) and solvothermal (c, d), respectively

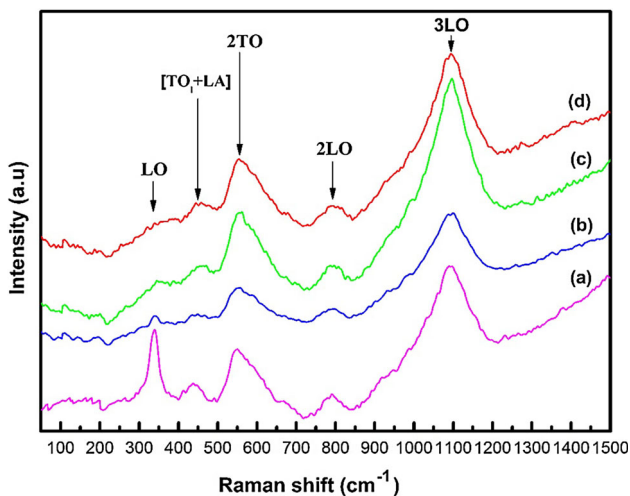


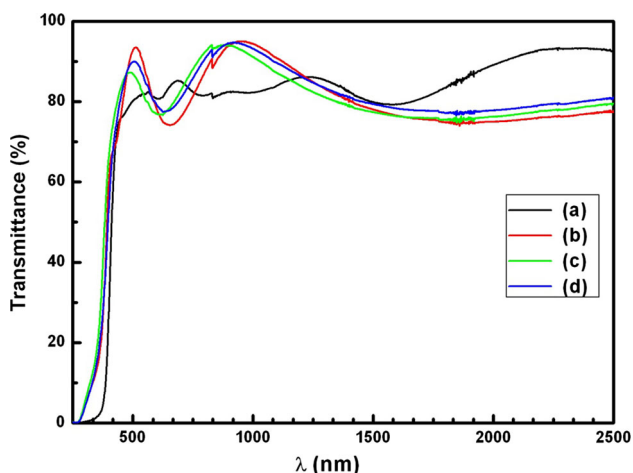
**Fig. 6** Raman spectra of ZnS thin films deposited at RT (a, c) and 200 °C (b, d) from nanoparticles elaborated by hydrothermal (a, b) and solvothermal (c, d), respectively

2LO mode. The well resolved peak at  $1093\text{ cm}^{-1}$  is also observed for all samples. This peaks at about  $1093\text{ cm}^{-1}$  is related to the longitudinal optical (3LO) phonon of ZnS. In addition to the strong peak at  $1093\text{ cm}^{-1}$ , the Raman spectra also show weak peak at about  $441\text{ cm}^{-1}$ . With regard to the  $441\text{ cm}^{-1}$  peak, it can be assigned to the  $[\text{TO}_1 + \text{LA}]_{\Sigma}$  mode. The Raman phonon modes  $[\text{TO}_1 + \text{LA}]_{\Sigma}$  and 3LO reported by Raman spectra were in good agreement with the literature [30, 31].

The high transparency is the most important factor in the application of thin films as buffer layer in solar cells. The optical properties of ZnS thin films are determined from transmittance and absorbance measurements in the range 200–2500 nm. The resulting transmittance spectra of ZnS thin films deposited at room temperature and 200 °C are shown in Fig. 7. They show interference fringes due to the multiple reflections at the interfaces; their observation indicates a fairly homogeneous film thickness. All these

**Table 3** The position of Raman peaks

Samples	LO (cm <sup>-1</sup> )	[TO <sub>1</sub> + LA] <sub>Σ</sub> (cm <sup>-1</sup> )	2TO (cm <sup>-1</sup> )	2LO (cm <sup>-1</sup> )	3LO (cm <sup>-1</sup> )
(a)	340	441	549	790	1093
(b)	340	441	549	790	1093
(c)		449	551	791	1097
(d)		449	551	791	1097

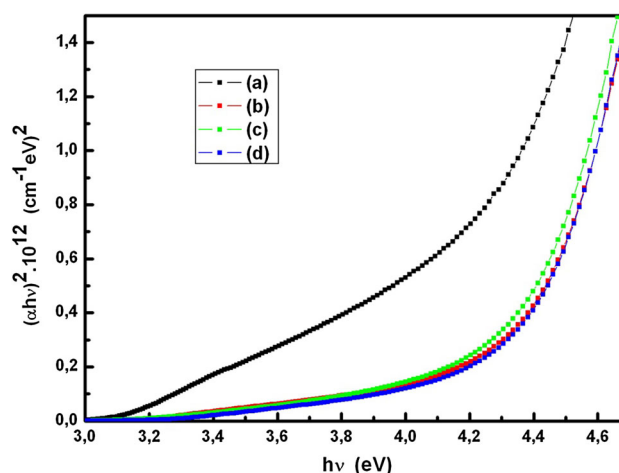
**Fig. 7** Optical transmittance of ZnS thin films prepared at RT (*a, c*) and 200 °C (*b, d*) from nanoparticles elaborated by hydrothermal (*a, b*) and solvothermal (*c, d*), respectively

sputtered films show an excellent transparency within the visible range (350–850 nm) with an average transmittance of about 90 %. The transmittance falls sharply at the band edge which is an indication of the good films crystallinity and low defect density near the band edge [32].

For a direct band gap semiconductor, the optical band gap energy ( $E_g$ ) can be estimated from the absorption spectrum ( $\alpha h\nu$ ) using the following relation [33]:

$$\alpha(h\nu) = C(h\nu - E_g)^{1/2} \quad (2)$$

where  $\alpha$  is the optical absorption coefficient,  $h\nu$  is the incident photon energy and  $C$  is a constant for direct transition. Figure 8 shows the plots of  $(\alpha h\nu)^2$  versus photon energy ( $h\nu$ ) for all samples. The optical energy gap ( $E_g$ ) of the films are obtained by extrapolating the straight portion of the graph on the  $h\nu$  axis at  $\alpha = 0$ . The estimated band gap values are listed in Table 2. Similar results are also reported by others [34]. Our band gap values of the sputtered ZnS thin films are somewhat larger than the typical value of the bulk ZnS (3.6 eV), which could be attributed to quantum confinement effects due to the small grain size of the polycrystalline ZnS films [34, 35]. These higher values may be due to the formation of fine grains [35]. Another strong possibility, is explained by the combined effects of phonon and inhomogeneity broadening along with optical loss due to light scattering at the

**Fig. 8** Plots of  $(\alpha h\nu)^2$  versus photon energy  $h\nu$  of ZnS thin films prepared at RT (*a, c*) and 200 °C (*b, d*) from nanoparticles elaborated by hydrothermal (*a, b*) and solvothermal (*c, d*), respectively

nanocrystallites [36, 37]. The origin of the broadening due to inhomogeneity is generally ascribed to the fluctuation in the shape and size of the grains in the film and to the variation of the absorption peak corresponding to band to band transition [24, 38].

## 4 Conclusion

In this paper, thin layers of ZnS were successfully deposited on glass substrates by rf-magnetron sputtering process using nanopowders prepared by solvothermal/hydrothermal route, for the first time. Hence, we present a new technique for ZnS thin films produced by a low-cost process. Structural and optical properties of the thin films were investigated to explore the possibility of producing buffer layers of nanostructured ZnS through low-cost process. The structure of the films and nanoparticles has been specified by XRD, EDS, TEM microscope and AFM imaging. Also, Raman, transmittance and band gap energy were determined for deposited ZnS on glass substrate. ZnS nanoparticles with a grain size between 10 and 18 nm were obtained by simple solvothermal/hydrothermal technique. According to these results, ZnS thin films on glass have high quality and their average surface roughness was very low for films synthesized by hydrothermal technique. The

surface looked smooth; a roughness of the ZnS thin film on glass substrate is about 2 nm. This is an advantage of sputtering for deposited ZnS thin films from the other techniques. According to XRD data and Raman spectroscopy the ZnS thin films produced on glass substrate were polycrystalline, with a cubic structure. From optical study the films are highly transparent in the visible wavelength region with a sharp fundamental absorption edge and an average transmittance of about 90 %. ZnS grown by rf-magnetron sputtering directly from nanopowder films might be a promising candidate as buffer/window layer in CuInGaSe<sub>2</sub> and related thin film solar cells.

## References

- I.K. Sou, Z.H. Ma, Z.Q. Zhang, G.K.L. Wong, *J. Appl. Phys. Lett.* **76**, 1098 (2000)
- Y. Kavanagh, M.J. Alam, D.C. Cameron, *Thin Solid Films* **447**, 85 (2004)
- C. Jin, H. Kim, H.W. Kim, C. Lee, *J. Lumin.* **516**, 130 (2010)
- T. Nakada, M. Hongo, E. Hayashi, *Thin Solid Films* **431**, 242 (2003)
- B. Asenjo, A.M. Chaparro, M.T. Gutiérrez, J. Herrero, J. Klaer, *Sol. Energy Mater. Sol. Cells* **92**, 302 (2008)
- M.M. Islam, S. Ishizuka, A. Yamada, K. Sakurai, S. Niki, T. Sakurai, K. Akimoto, *Sol. Energy Mater. Sol. Cells* **93**, 970 (2009)
- J. Fang, H.P. Holloway, E.J. Yu, S.K. Jones, B. Pathangey, E. Brett Schneider, *J. Appl. Surf. Sci.* **701**, 70 (1993)
- J.A. Ruffner, M.D. Hilmel, V. Mizrahi, G.I. Stegeman, U. Gibson, *J. Appl. Opt.* **28**, 5209 (1989)
- A.M. Ledger, *Appl. Opt.* **18**, 2979 (1979)
- D. Schmid, M. Ruckh, H.W. Schock, *Sol. Energy Mater. Sol. Cells* **281**, 41 (1996)
- T. Wada, Y. Hashimoto, S. Nashiwaki, T. Satoh, *Sol. Energy Mater. Sol. Cells* **67**, 305 (2001)
- J.M. Dona, J. Herrero, *J. Electrochem. Soc.* **141**, 205 (1994)
- A. Ennaoui, W. Eisele, M. Lux-Steiner, T.P. Niesen, F. Karg, *Thin Solid Films* **431**, 335 (2003)
- R.N. Bhattacharya, K. Rammanathan, *Sol. Energy* **77**, 679 (2004)
- G.D. Brownlie, B. Voegle, W. Meredith, J.S. Milnes, K.A. Prior, B.C. Cavenett, *J. Cryst. Growth* **37**, 184 (1998)
- C.T. Hsu, *Mater. Chem. Phys.* **58**, 6 (1999)
- A. Ganguly, S. Chaudhuri, A.K. Pal, *J. Phys. D Appl. Phys.* **34**, 506 (2001)
- J.H. Song, E.D. Sim, K.S. Back, S.K. Chang, *J. Cryst. Growth* **460**, 214 (2000)
- Y. Zhao, Y. Zhang, H. Zhu, G.C. Hadjipanayis, J.Q. Xiao, *J. Am. Chem. Soc.* **126**, 6874 (2004)
- F. Huang, J.F. Banfield, *J. Am. Chem. Soc.* **127**, 4523 (2005)
- B.D. Cullity, *Elements of X-Ray Diffraction* (Addison-Wesley, Reading, MA, 1978), p. 102
- Y.P. Venkata Subbaiah, P. Prathap, K.T. Ramakrishna Reddy, *Appl. Surf. Sci.* **253**, 2409 (2006)
- D. Yoo, M.S. Choi, S.C. Heo, C. Chung, D. Kim, C. Choi, *Met. Mater. Int.* **19**, 1309 (2013)
- P. Chelvanathan, Y. Yusoff, F. Haquea, M. Akhtaruzzaman, M.M. Alam, M.J. Rashid, K. Sopian, N. Amin, *Appl. Surf. Sci.* **334**, 138 (2015)
- H. Kina, Y. Yamada, Y. Maruta, Y. Tamura, *J. Cryst. Growth* **169**, 33 (1996)
- S.B. Qadri, E.F. Skelton, D. Hsu, A.D. Dinsmore, J. Yang, H.F. Gray et al., *Phys. Rev. B* **60**, 13 (1999)
- J.F. Vetelinot, S.S. Mitra, O. Brafman, S.S. Mitra, *Phys. Rev. B* **7**, 1809 (1969)
- Y.C. Cheng, C.Q. Jin, F. Gao, X.L. Wu, W. Zhong, S.H. Li, Paul.K. Chu, *Appl. Phys.* **106**, 123505 (2009)
- J. Serrano, A. Cantarero, M. Cardona, N. Garro, R. Lauck, R.E. Taliman, T.M. Ritter, B.A. Weiastein, *Phys. Rev. B* **69**, 014301 (2004)
- Y.J. Zhang, C.S. Xu, Y.C. Liu, Y.X. Liu, G.R. Wang, X.W. Fan, *J. Lumin.* **119–120**, 242 (2006)
- F. Göde, *Phys. B* **406**, 1653 (2011)
- J. Cheng, D.B. Fan, H. Wang, B.W. Liu, Y.C. Zhang, H. Yan, *Semicond. Sci. Technol.* **18**, 676 (2003)
- J.I. Pankove, *Optical Processes in Semiconductors* (Dover, New York, 1976), p. 91
- P.K. Ghosh, S. Jana, S. Nandy, K. Chattopadhyay, *Mater. Res. Bull.* **42**, 505 (2007)
- P.K. Ghosh, M.K. Mitra, K.K. Chattopadhyay, *Nanotechnology* **16**, 107 (2005)
- S. Schmitt-Rink, D.A.B. Miller, D.S. Chemla, *Phys. Rev. B* **35**, 8113 (1987)
- R. Pal, D. Bhattacharyya, A.B. Maity, S. Chaudhuri, A.K. Pal, *Nanostruct. Mater.* **4**, 329 (1994)
- S.K. Mandal, S. Chaudhuri, A.K. Pal, *Thin Solid Films* **350**, 209 (1999)